Journal of Catalysis 265 (2009) 8–18

Contents lists available at ScienceDirect

Journal of Catalysis

journal homepage: www.elsevier.com/locate/jcat

Dynamics of redox behavior of nano-sized VO_x species over Ti–Si-MCM-41 from time-resolved in situ UV/Vis analysis

Olga Ovsitser, Maymol Cherian, Angelika Brückner, Evgenii V. Kondratenko *

Leibniz-Institut für Katalyse e. V. an der Universität Rostock, Albert-Einstein-Str. 29a, D-18059 Rostock, Germany

ARTICLE INFO

Article history:
Received 5 February 2009
Revised 1 April 2009
Accepted 3 April 2009
Available online 9 May 2009

Dedicated to Professor Dr. Manfred Baerns on the occasion of his 75th birthday.

Keywords:
In situ UV/Vis
Vanadia
Silica
Titanium
Propane
Propene
ODP
N_2O
Reaction mechanism

ABSTRACT

Time-resolved in situ UV/Vis spectroscopy has been successfully applied for analyzing the reduction degree of highly dispersed VO_x (0.4–1.1 V/nm^2) species over Ti–Si-MCM-41 (Ti/Si = 0–1.5) materials in the oxidative dehydrogenation of propane (ODP) as well as for deriving the kinetic parameters of reduction (with C_3H_8) and reoxidation (with O_2 and N_2O) of these species. This quantitative kinetic study enabled to recognize at least two types of differently reducible VO_x species in the samples with titanium. Three effects of titanium on redox properties of VO_x species were identified: (i) the constant of reduction of oxidized VO_x species by C_3H_8 increases, (ii) the constant of oxidation of reduced VO_x species by O_2 decreases; and (iii) the constant of oxidation of reduced VO_x species by N_2O increases. These effects are highly relevant for the ODP performance. The intrinsic ODP activity increases linearly with an increase in the constant of reduction of oxidized VO_x species. Propene selectivity is determined by the ratio of the constants of reduction and reoxidation of VO_x species; the higher the ratio, the higher the selectivity. This ratio can be tuned by the oxidizing agent (O_2 vs. N_2O) and by the Ti/Si ratio.

1. Introduction

Monitoring the events taking place over catalytic materials under real reaction conditions is crucial for elucidating the reaction mechanisms, and for establishing the relationships between catalytic performance (reactivity/selectivity) and physico-chemical properties of the catalysts. This knowledge is of great importance for the rational design of new or improved catalytic materials. UV/Vis spectroscopy nowadays is one of a very few methods for characterizing heterogeneous catalysts under their working conditions [1–8]. When combining it with mass-spectroscopic and/or gas-chromatographic analysis, the state of catalytic materials, their activity, and selectivity can be simultaneously determined in one reactor system [9]. As a result, problems arising from differences in reaction conditions and cell designs are avoided. Therefore, a direct link between the physico-chemical and catalytic properties can be established.

UV/Vis spectroscopy in different modifications has been applied to investigate the extent of reduction of VO_x species under different reaction conditions [5,7,10–12]. To our best knowledge, only a couple of studies has been aimed to analyze the kinetics of reduction and reoxidation of active surface species by in situ UV/Vis spectroscopy. The kinetics of reduction of CrO_3 by CO has been investigated in [13]. Kinetic parameters of reduction of VO_x/MCM-41 by hydrogen have been determined in [14]. Argyle et al. [15] have monitored the dynamics of reduction of VO_x species over Al_2O_3 with propane from transient analysis of UV/Vis spectra in the near-edge region. In situ UV/Vis spectroscopic study in the range of d–d transitions of reduced VO_x species enabled to determine redox kinetics of VO_x species in VO_x/TiO_2 catalysts used in oxidative scission of butane to acetic acid [16]. Two different processes, a fast one and a slow one, have been identified and attributed to reduction/reoxidation of VO_x species on the outer surface and in the subsurface layers. Very recently, UV/Vis spectroscopy was combined with in situ X-ray absorption near-edge spectroscopy (XANES) to determine the temporal evolution of coverage by hydroperoxo species over gold/titanosilicalite catalysts in the propane oxidation with H_2 and in the propylene epoxidation [17,18]. Moreover, these authors have demonstrated that the reaction rates determined by XANES were close to the turnover rates measured in a catalytic flow reactor, indicating that the hydroperoxo species were true intermediates in these reactions. In our previous study [11], we have qualitatively demonstrated that the reduction of VO_x species

* Corresponding author. Fax: +49 381 1281 51290.
E-mail address: evgenii.kondratenko@catalysis.de (E.V. Kondratenko).

0021-9517/$ - see front matter © 2009 Elsevier Inc. All rights reserved.
doi:10.1016/j.jcat.2009.04.005

over MCM-41 with C_3H_8 is slower than their reoxidation with O_2 by performing C_3H_8 and O_2 switch experiments with simultaneous in situ UV/Vis analysis at 773 K.

The present contribution reports on the kinetics of reduction and reoxidation of VO_x species by C_3H_8 and $O_2(N_2O)$, respectively, as derived from quantitative evaluation of time-resolved UV/Vis measurements in the range of d–d transitions of reduced VO_x species. In order to evaluate the sensitivity of this approach to the effect of the support on the redox properties of highly dispersed surface VO_x species, VO_x(3.7 wt.%)/(Ti–Si)O_2 materials with different titanium loadings were prepared and applied for the oxidative dehydrogenation of propane (ODP). The catalysts were chosen considering the following knowledge. $V_2O_5/TiO_2/SiO_2$ materials demonstrate excellent catalytic performance in selective catalytic reduction [19], selective oxidation of ortho-xylene [20], ethanol [21] and propane oxidative dehydrogenation [22]. Whereas V_2O_5/TiO_2 is known as a very active, but not selective catalyst [23], the use of titania-silica supports, in which titanium oxide is highly dispersed and strongly interacting with the silica support, results in different catalytic characteristics compared to that of pure titania in the oxidative dehydrogenation of ethane [24]. Higher selectivity and activity to ethylene were observed over $V_2O_5/TiO_2/SiO_2$ than over V_2O_5/SiO_2. According to our previous work [11], time-resolved UV/Vis spectroscopic measurements were carried out in a fixed bed continuous flow reactor under real catalytic conditions called "operando" [1,25] using an in-house developed reactor system (Fig. 1) combined with on-line mass-spectroscopic and gas-chromatographic analysis. In order to avoid any misinterpretation of UV/Vis measurements, particular attention was paid to control C_3H_8, and O_2/N_2O conversion as well as reaction temperature inside the catalyst bed. The obtained results helped to understand the factors governing the superior performance of N_2O compared to that of O_2 in the selective oxidation of propane to propene over vanadia-based catalysts [11,26,27].

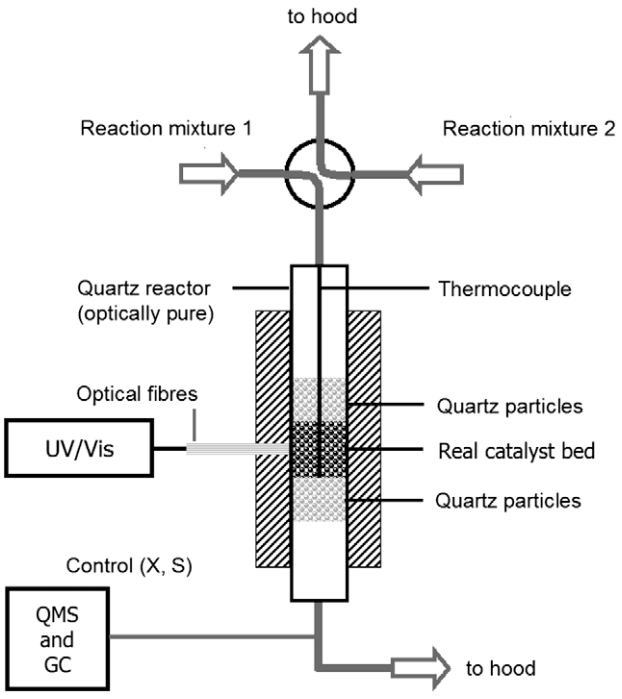

Fig. 1. Schematic representation of an in-house developed set-up for simultaneous catalytic testing and catalyst characterization by in situ UV/Vis spectroscopy.

2. Experimental

2.1. Preparation of catalytic materials

A series of $VO_x/(Ti–Si)O_2$ materials with a total vanadium loading of ca. 3.7 wt.% and a Ti/Si ratio varying from 0 to 1.5 was prepared. The mesoporous support materials were prepared according to [14,27,28]. The vanadium-containing catalysts were synthesized by impregnating the support with pre-defined amounts of vanadyl acetyl acetate dissolved in toluene followed by sample flushing in toluene. This preparation method leads to highly dispersed surface VO_x species. The resulting catalyst precursor was subsequently subjected to drying at 400 K for 12 h and calcination in air at 823 K for 12 h in a muffle furnace. The total amount of vanadium and titanium was determined after the calcination. Along the manuscript, the catalysts are denoted by their titanium to silicon ratio in the support; e.g. VO_x(3.7 wt.%)/(Ti–Si)O_2 (Ti/Si = 1.5) will be referred to as V–TiSi-15 (Table 1).

2.2. Catalyst characterization

Nitrogen physisorption at 77 K was employed to obtain specific surface areas of the unloaded supports and the catalysts using single-point BET procedure (Gemini III 2375, Micromeritics).

Inductively coupled plasma (*ICP*) measurements were used to determine the concentration of vanadium, titanium, and silicon in the catalysts after calcination at 823 K.

X-ray diffraction (*XRD*) was carried out using a STADIP transmission powder diffractometer (Stoe) with $CuK_{\alpha 1}$ radiation.

EPR measurements of hydrated VO_x(3.7 wt.%)/(Ti–Si)O_2 (Ti/Si = 0–1.5) samples were performed at 77 K by using a c.w. spectrometer ELEXSYS 500-10/12 (Brucker) in X-band. The magnetic field was measured with respect to the standard 2,2–diphenyl-1-picrylhydrazyl hydrate.

H_2-TPR (temperature-programmed reduction) tests were carried out by heating the sample (100 mg) with a heating rate of 20 K/min up to 1073 K in a flow of 10 vol.% H_2 in Ar with a total flow rate of 50 cm^3_{STP} min^{-1}. The H_2 consumption was determined using a thermal conductivity detector. Water formed or desorbed during the TPR measurements was removed by molecular sieve 4 Å before the flow entered the detector. The hydrogen concentration was calibrated by argon pulses continuously introduced into the gas flow during sample heating.

Laser Raman spectra of powder samples (10–20 mg) were collected using a Kaiser Optical Systems RXN spectrometer with excitation at 785 nm. They were recorded at room temperature after dehydration of catalytic materials at 723 K in flowing oxygen (O_2/He = 20/80) in an environmental cell (Linkam, model T1600).

In situ UV/Vis experiments were performed under steady-state and transient conditions using an AVASPEC fiber optical spectrometer (Avantes) equipped with a DH-2000 deuterium-halogen light source and a CCD array detector. $BaSO_4$ was used as a white refer-

Table 1
Surface and bulk properties for unloaded (Ti–Si)O_2 supports and $VO_x/(Ti–Si)O_2$ materials.

Sample	V (wt.%)	Ti/Si	S_{BET} (m^2 g^{-1})	V surface density (V/nm^2)
TiSi-0	–	0	1011	–
V–TiSi-0	2.7	0	871	0.37
TiSi-1		0.12	769	–
V–TiSi-1	3.5	0.12	703	0.59
TiSi-6		0.64	746	–
V–TiSi-6	3.9	0.64	698	0.66
Ti–Si-15		1.5	621	–
V–TiSi-15	3.8	1.5	413	1.1

ence material. A high-temperature reflection UV/Vis probe consisting of 6 radiating optical fibers and 1 reading one was located inside the furnace perpendicular to the reactor (Fig. 1). In contrast to the usually used stainless steel spectroscopic reactors with spectroscopic quartz windows [1,13], our whole reactor was made of pure spectroscopic quartz. Another advantage of this reactor system is that the possible blind activity of the reactor is nearly completely suppressed. Moreover, reaction temperature within the fixed bed of catalyst particles was controlled by an axially movable thermocouple located inside a capillary made of quartz. The reflection UV/Vis probe was connected to the spectrometer and the light source by fiber optical cables consisting of a core of pure silica (diameter 0.4 mm) coated with polyimide. The spectra were converted into the Kubelka–Munk function $F(R)$. It is important to emphasize that the position of the UV/Vis fiber, the total flow, the reaction temperature, and the overall pressure were not changed upon switching between various reaction feeds. Therefore, the observed changes in the UV/Vis spectra relate exclusively to the change(s) of the catalyst under different reaction conditions.

In steady-state UV/Vis experiments, UV/Vis spectra were recorded in the range of 200–800 nm under different reactive flows (C_3H_8/O_2/Ne = 40/20/40, and C_3H_8/N_2O/Ne = 40/40/20) at 773 K. Steady-state UV/Vis spectra were recorded 10 min after switching to the respective flow.

In transient UV/Vis experiments, UV/Vis spectra (from 200 to 800 nm) and the Kubelka–Munk function at 700 nm (d–d-transitions of reduced V-species) were recorded every 5 s under different reaction conditions (C_3H_8/Ne = 40/60, H_2/N_2 = 5/95, N_2O/Ne = 40/60 and O_2/Ne = 20/80). The temporal changes in the Kubelka–Munk function at 700 nm are related to the kinetics of reduction of oxidized VO_x species and reoxidation of reduced VO_x species upon feeding reducing and oxidizing flows, respectively. It is accepted that the Kubelka–Munk function of weakly absorbing samples is linearly related to the absorbance and, thus, to the number of absorbing species when it is smaller than 0.5 [29]. This condition is fulfilled for $F(R)$ values at 700 nm used for the kinetic evaluation in this work.

In both modes, UV/Vis spectra were taken at 773 K by passing reactive mixtures through the catalyst bed. The total gas flow was kept at 40 cm^3_{STP} min^{-1}. Catalyst particles of 0.1–0.2 mm were used for these investigations. All these experimental conditions including the quartz-made reactor were very similar to those in standard catalytic continuous flow tests. The catalyst was sandwiched between the two layers of quartz particles (0.25–0.35 mm) to fix the catalyst, to pre-heat the reaction feed, and to minimize the dead volume of the reactor in the hot zone. In order to keep the conversion of propane and oxidant (O_2/N_2O) below 10% and 20% under the ODP conditions, and to ensure isothermal operation, catalyst particles (3–5 mg) were diluted with quartz particles. Undiluted catalysts (20–30 mg) were used to study the kinetics of reduction and oxidation of oxidized and reduced VO_x species under C_3H_8(H_2) and O_2(N_2O) feeds, respectively. The gas composition at the reactor outlet during the in situ UV/Vis experiments was controlled by on-line mass spectrometry (Balzer Omnistar). The propane and oxidant (O_2, N_2O) conversion was calculated from the inlet and outlet concentrations of these components.

2.3. Steady-state continuous flow catalytic tests

The oxidative dehydrogenation of propane (ODP) was investigated in a U-shaped fixed-bed quartz reactor (i.d. 5 mm) at 1 bar and 773 K using C_3H_8/N_2O/Ne = 40/40/20 and C_3H_8/O_2/Ne = 40/20/40 reaction feeds. The reactor was immersed into a fluidized bed of quartz sand to provide isothermal operating conditions. A movable thermocouple inside the reactor was used to control temperature inside the catalyst bed. In order to determine product selectivity at different degrees of propane conversion, the total flow rate and the catalyst amount were varied from 20 to 240 cm^3_{STP} min^{-1}, and from 0.003 to 0.2 g, respectively. The product mixture was analyzed using on-line GC (HP 5890-II) equipped with Porapak Q and Molecular sieve 5 columns. The conversion of feed components, selectivity and yield of reaction products were calculated from the inlet and outlet concentrations considering the changes of reaction volume during the ODP reaction. In order to determine the overall rate of propane consumption, the propane conversion was kept below 2%, i.e. the catalytic reactor can be considered as a differential one, and any influence of reaction products on the rates measured is minimized. The degree of O_2 and N_2O conversion under these conditions was always below 10%. The overall rate was used to calculate the turnover frequencies (TOF) according to Eq. (1). The TOF values represent the number of propane molecules converted over one V atom per second. Since the results of catalyst characterization in Section 3.1 suggest the presence of only highly dispersed VO_x species (no three-dimensional VO_x aggregates), it is reasonable to assume that all VO_x species are exposed to the reaction feed and are active for C_3H_8 oxidation.

$$\mathrm{TOF} = \frac{r_{C_3H_8}}{n_V} \tag{1}$$

where $r_{C_3H_8}$ is the rate of propane conversion (number of propane moles converted per gram of catalyst per second), and n_V is the number of moles of vanadium per gram of catalyst (mol(V)/g).

Catalytic activity and product selectivity changed during first 0.5–1.5 h on stream. After this time, a steady-state operation was achieved. Therefore, the concentration of reaction products and feed components after 1.5–2 h on stream was taken for calculation of reaction rates, conversion, and selectivity.

3. Results and discussion

The following section describes the results of physico-chemical characterization of the VO_x/(Ti–Si)O_2 catalytic materials. The catalytic performance of these materials in the ODP reaction in the presence of O_2 and N_2O is subsequently presented. Hereafter, the kinetics of reduction and oxidation of VO_x species is described from the results of time-resolved in situ UV/Vis analysis under reducing (C_3H_8/Ne = 40/60 and H_2/N_2 = 5/95) and oxidizing (N_2O/Ne = 40/60 and O_2/Ne = 20/80) conditions. Finally, the results derived are discussed together to explain the effect of Ti and N_2O on the ODP performance of VO_x/(Ti–Si)O_2 catalysts.

3.1. Influence of titanium on surface and bulk properties of VO_x/(Ti–Si)O_2

Table 1 summarizes apparent surface densities of vanadium, chemical composition (from ICP analysis), and specific surface areas (S_{BET}) of pure supports, and VO_x/(Ti–Si)O_2 materials. The surface areas of the supports decreased from ca. 1000 to ca. 600 m^2 g^{-1} upon increasing the ratio of Ti/Si from 0 to 1.5. Additionally, the BET values of the catalysts are further reduced by ca. 7–30% after impregnation of the supports with VO_x species (Table 1). The decrease in the surface areas of the vanadium-impregnated samples is due to the plugging of pores. The strongest negative effect of impregnation on the BET surface was observed for the V–TiSi-15 sample. This may be due to the fact that the unloaded TiSi-15 support had the lowest BET surface area among the other unloaded supports. Using these BET values and vanadium loading, apparent surface densities of vanadium (V/nm^2) were calculated and are in the range of 0.4–1.1 V/nm^2. Taking into account such values reported in [30], it can be safely concluded that our catalytic materials mainly possess VO_x species significantly below one vanadium monolayer, i.e. 0.04–0.15 vanadium monolayer.

Independent of Ti loading, the EPR spectra of hydrated VO_x species in Fig. 2 show the characteristic hyperfine splitting multiplet of well-isolated octahedrally coordinated V^{4+} species [31]. However, the hyperfine structure signal of truly isolated VO^{2+} species in V–TiSi-15 is superimposed by a broad singlet. This points to the presence of a minor amount of small VO_x clusters consisting of a few V atoms only (by far too small to be detectable by XRD or Raman spectroscopy) in this material. In summary, we can conclude that all the samples irrespective of titanium loading mainly possess highly dispersed VO^{2+} species.

Laser Raman spectroscopy was applied in order to obtain more detailed information about the possible presence of XRD-amorphous V_2O_5 nanoparticles and the distribution of surface VO_x species. Since nano-sized V_2O_5 species can be easily detected under visible excitation [32], the Raman spectra were collected at 785 nm excitation. The Raman spectra of the V–TiSi-1 and V–TiSi-15 catalysts are compared in Fig. 3. The absence of a sharp Raman band at 990–994 cm^{-1} demonstrates that crystalline V_2O_5 nanoparticles are not present in all the samples. The band at ~1022 cm^{-1} can be associated with dehydrated, highly dispersed surface O=V(–O–Me–)$_3$ species [32–34], where Me is Si or Ti. However, recent theoretical and experimental studies on the Raman spectra of VO_x/SiO_2 provide an indication that the band at 1000–1030 cm^{-1} cannot be exclusively assigned to vanadyl species but can belong to V–O–Si vibrations [35].

In order to investigate the effect of titanium in the support on the reducibility of surface VO_x species, H_2-TPR tests were performed. The obtained temperature-programmed profiles of hydrogen consumption over the $VO_x/(Ti–Si)O_2$ materials are presented in Fig. 4. It should be particularly stressed that no significant H_2 consumption was observed over the bare supports. Therefore, the TPR results discussed below are due to the reduction of surface VO_x species. Independent of Ti loading, the H_2-TPR profiles over all the materials are characterized by a maximum of H_2 consumption (T_{max}) at 803–810 K (Fig. 4). The single T_{max} obtained for the V–TiSi-0 sample represents a single-stage reduction of V^{5+} to V^4/V^{3+} supported over SiO_2 [36,37]. The H_2-TPR profiles over the Ti-containing samples possess an additional shoulder with a maximum shifted to lower temperatures. This is due to the presence of easily reducible VO_x species, which are probably bound to titanium [38]. Since the results of H_2-TPR tests demonstrate that the reducibility

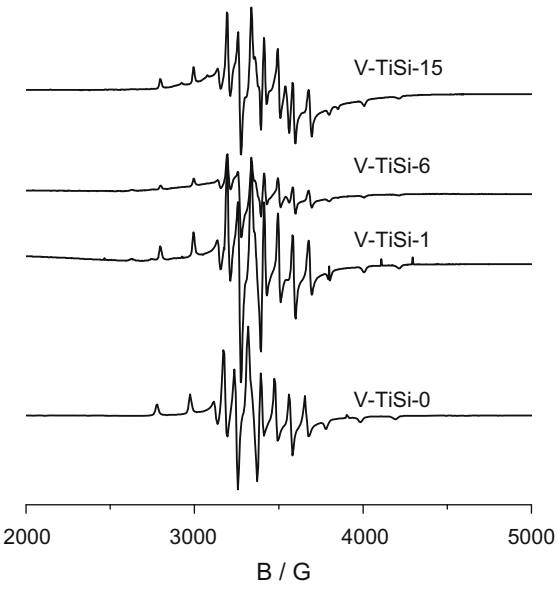

Fig. 2. EPR spectra of $VO_x/(Ti–Si)O_2$ catalysts at 77 K.

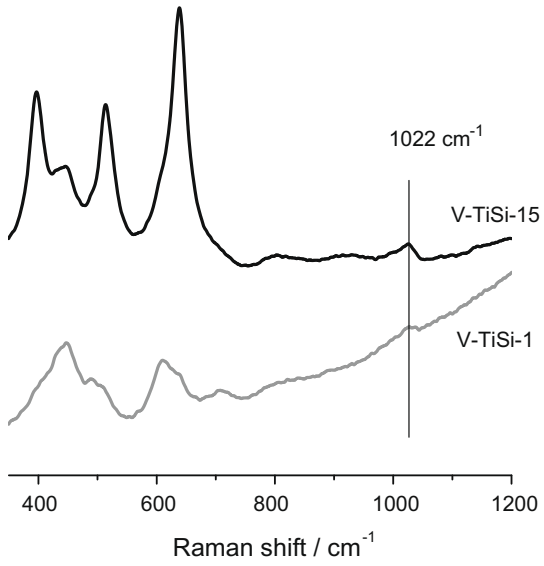

Fig. 3. Raman spectra of V–TiSi-1 and V–TiSi-15 catalysts under dehydrated conditions with 785 nm excitation wavelengths.

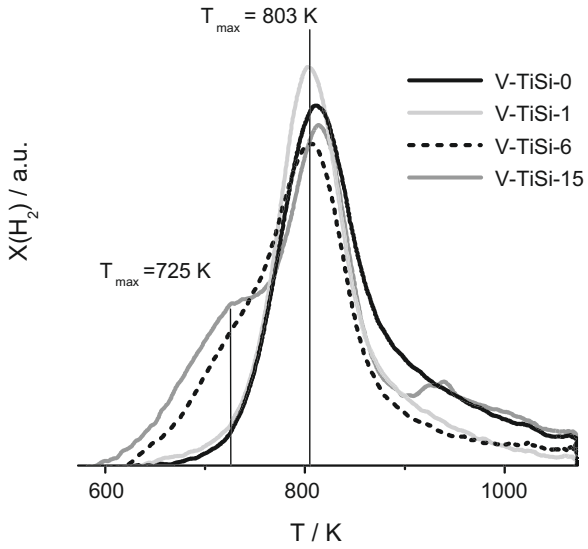

Fig. 4. Temperature-programmed reduction profiles of $VO_x/(Ti–Si)O_2$ catalysts.

of VO_x increases with Ti loading, we suggest that Ti weakens the strength of V–O bond(s) in the VO_x species connected to TiO_x. The TPR pattern of V–TiSi-15 (Fig. 4) also possesses a low-intensity maximum of H_2 consumption at ca. 930 K. For the TiSi-15 support, we observed a maximum of H_2 consumption at ca. 890 K. Therefore, this TPR signal suggests the presence of hardly reducible VO_x or TiO_x species. Since the ODP reaction was investigated at 773 K, we assume that the latter species do not participate in the ODP reaction.

3.2. Catalytic performance of $VO_x/(Ti–Si)O_2$ with O_2 and N_2O

Catalytic performance (turnover frequencies and selectivity-conversion relationship) of $VO_x/(Ti–Si)O_2$ samples was determined at 773 K using $C_3H_8/O_2/Ne$ = 40/20/40 and $C_3H_8/N_2O/Ne$ = 40/40/20 reaction feeds. Since the amount of N_2O was twice that of O_2, both reaction feeds contained the same amount of oxygen atoms. This allows the comparison of the influence of oxidizing agents on the

ODP reaction. For all the materials, C_3H_6 selectivity decreases with an increase in C_3H_8 conversion with both N_2O and O_2 (Fig. 5), while CO and CO_2 selectivity increases (the data are not shown for brevity). This means that propene primarily formed from propane is consecutively oxidized to carbon oxides. However, it should be especially highlighted that the decrease in propene selectivity is significantly influenced by the ratio of Ti/Si in the catalysts, and by the oxidizing agent. As defined in our previous paper [11], the slope of the dependence of propene selectivity on propane conversion represents the catalyst activity for consecutive propene oxidation; the lower is the slope, the lower is the activity. The lowest slope was obtained for the sample without titanium, while the highest one was determined for the V–TiSi-15 material. Another important result is that the improving effect of N_2O on C_3H_6 selectivity depends on the Ti/Si ratio. Fig. 5 clearly demonstrates that C_3H_6 selectivity over V–TiSi-0 is higher and decreases slower with increasing C_3H_8 conversion using N_2O than O_2. The difference in the C_3H_6 selectivity between N_2O and O_2 decreases with an increase in the Ti loading. Although Ti increases consecutive C_3H_6 oxidation with O_2 and N_2O, Ti positively influences the initial C_3H_6 selectivity (extrapolated to zero degree of C_3H_8 conversion), when O_2 is used as an oxidizing agent. The highest initial C_3H_6 selectivity (ca. 95%) in the O_2-containing feed was observed over the V–TiSi-15 catalyst possessing the highest Ti loading (Fig. 5). A possible explanation of the Ti effect of the propene selectivity is given in Section 3.4 taking into account the results of in situ UV/Vis analysis given in Section 3.3.

The presence of Ti in the support materials influences also the turnover frequency (TOF) of propane conversion in the ODP reaction over the $VO_x/(Ti–Si)O_2$ catalysts. Fig. 6 shows that the TOF values with O_2 increase by a factor of ca. 20 upon increasing the Ti/Si ratio from 0 to 1.5. When N_2O was used as an oxidant, the TOF values increased only by a factor of ca. 5 (Fig. 6). It should be stressed at this point that all our samples possess similar vanadium loading of 3.7 wt.%. Therefore, the increase in the catalytic activity with Ti loading should be related to the changes in the properties of VO_x species [39], since the unloaded supports are significantly less active than the catalysts. The following in situ UV/Vis spectroscopic analysis is aimed to answer why the presence of Ti in the support increases the overall catalytic activity and influences the selectivity-conversion relationship of the ODP reaction.

3.3. In situ UV/Vis analysis of redox behavior of VO_x species

In order to prove if possible reduction of TiO_2 in H_2 and C_3H_8 (10 vol.% H_2 in Ar and 40 vol.% C_3H_8 in Ne) at 773 K contributes to any changes in UV/Vis spectra, we performed UV/Vis tests with the unloaded support possessing the highest Ti content (TiSi-15). The absorption in the 600–800 nm range (d–d transitions of reduced species) increased upon switching from the oxidative to the reductive flow and can be related to the reduction of Ti^{4+} to Ti^{3+}. However, this increase was ca. 300 times lower compared to that in the vanadium-containing samples. This means that TiO_2 is significantly less reducible at 773 K than VO_x species. Therefore,

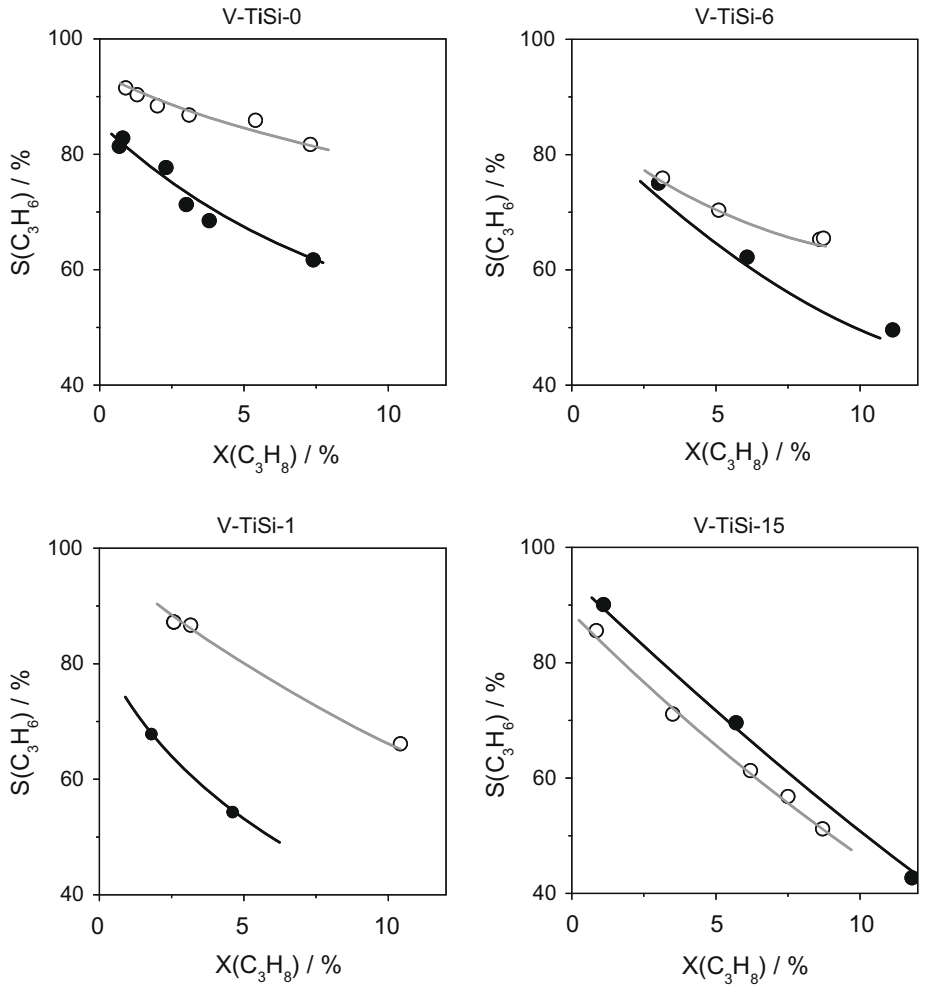

Fig. 5. Selectivity to propene as a function of propane conversion using $C_3H_8/O_2/Ne = 40/20/40$ (●) and $C_3H_8/N_2O/Ne = 40/40/20$ (○) mixtures at $T = 773$ K.

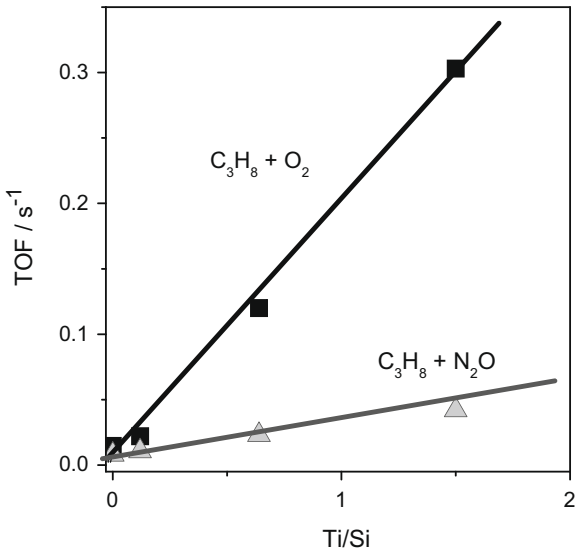

Fig. 6. Turnover frequency (TOF) of propane conversion as a function of Ti/Si ratio in the support. Reaction conditions: T = 773 K, $C_3H_8/O_2/Ne$ = 40/20/40, and $C_3H_8/N_2O/Ne$ = 40/40/20.

the changes in UV/Vis spectra discussed below are exclusively due to the redox properties of VO_x species.

3.3.1. Steady-state oxidation state of VO_x species under controlled ODP conditions

Steady-state UV/Vis measurements were performed at 773 K under continuous flow conditions (40 cm^3_{STP} min^{-1}) using different gas mixtures. The experimental set-up used in the present study allows to take UV/Vis spectra and to simultaneously measure the degrees of propane and oxidant (O_2 and N_2O) conversion by means of MS (mass-spectrometry) and GC (gas-chromatographic) analysis as well as to control the temperature inside the catalyst bed (Fig. 1). Here we would like to give an example illustrating the importance of such a control.

In preliminary experiments, in situ UV/Vis spectra of the V–TiSi-15 catalyst (20 mg) were recorded under $C_3H_8/O_2/Ne$ = 40/20/40 and $C_3H_8/N_2O/Ne$ = 40/40/20 flows at 773 K. Surprisingly, the UV/Vis spectrum in the $C_3H_8/O_2/Ne$ = 40/20/40 feed showed considerably higher Kubelka–Munk values in the range of 600–800 nm (d–d transitions of reduced VO_x species) than that in the C_3H_8/Ne = 40/60 flow. Based on these results, one can expect that the degree of reduction of VO_x species under $C_3H_8/O_2/Ne$ = 40/20/40 is higher than that under C_3H_8/Ne = 40/60. Moreover, the Kubelka–Munk values were lower under $C_3H_8/N_2O/Ne$ = 40/40/20 than in the $C_3H_8/O_2/Ne$ = 40/20/40 flow. However, when we checked the temperature inside the catalyst bed during the spectroscopic measurements, we observed a high increase in temperature (up to 850 K) upon catalyst being exposed to the $C_3H_8/O_2/Ne$ = 40/20/40 feed. This increase is due to the high conversion of propane and oxygen (~100%) resulting in high heat production, which could

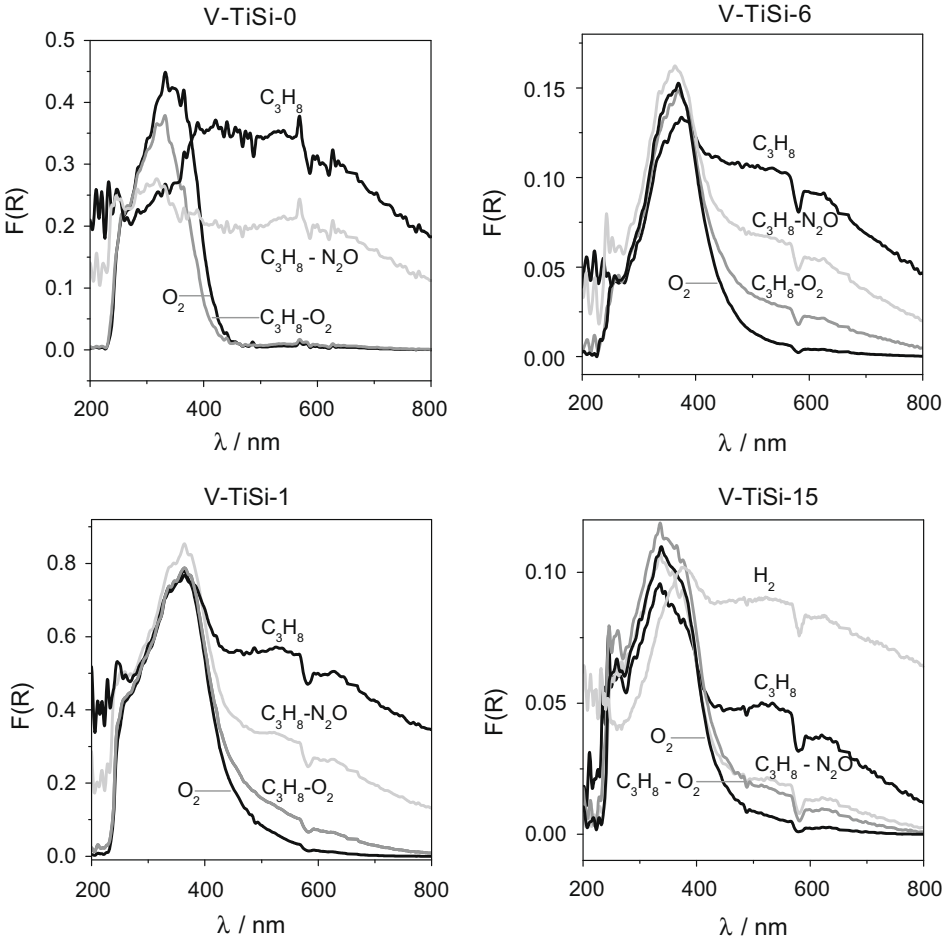

Fig. 7. In situ UV/Vis spectra of $VO_x/(Ti–Si)O_2$ (Ti/Si = 0–1.5) catalysts under isothermal reaction conditions at 773 K and controlled degrees of conversion; $X(C_3H_8)$ < 5%, $X(O_2)$, and $X(N_2O)$ < 10%.

not be effectively removed from the reactor. When the catalyst was exposed to a $C_3H_8/N_2O/Ne = 40/40/20$ flow, no temperature increase was observed. Moreover, in contrast to the near to complete O_2 conversion, the degree of N_2O conversion was lower than 20%. In summary, the UV/Vis spectrum of V–TiSi-15 in the $C_3H_8/O_2/Ne = 40/20/40$ flow does not represent the oxidation state of VO_x species at 773 K and in the presence of O_2 but it characterizes the oxidation state of VO_x species at 850 K and very high C_3H_8/O_2 ratio.

In order to avoid such a misinterpretation of the in situ UV/Vis spectra, we performed the following UV/Vis analysis using a lower amount of the V–TiSi-15 catalyst diluted additionally with SiO_2 particles. This experimental restriction was very essential to keep the conversion of feed components below 5–10% ensuring near to constant C_3H_8/O_2 (C_3H_8/N_2O) ratio along the catalyst bed and isothermal operation. Fig. 7 compares the UV/Vis spectra of V–TiSi-0, V–TiSi-1, V–TiSi-6, and V–TiSi-15 in oxidizing ($O_2/Ne = 20/80$), reducing ($C_3H_8/Ne = 40/60$) flows, and in the ODP ($C_3H_8/O_2/Ne = 40/20/40$ or $C_3H_8/N_2O/Ne = 40/40/20$) feeds at 773 K. For the V–TiSi-15 catalyst, the UV/Vis spectrum in a $H_2/N_2 = 5/95$ flow is additionally shown. It is clearly seen that the UV/Vis spectra in the H_2 and C_3H_8 flows are similar to each other. This important result proves that the changes observed in the UV/Vis spectra upon switching from O_2 to C_3H_8 or H_2 are due to the reduction of VO_x species but not due to coke deposition.

No significant differences in the UV/Vis spectra of V–TiSi-0 were observed during the ODP reaction with O_2 ($C_3H_8/O_2/Ne = 40/20/40$) and in an O_2 ($O_2/Ne = 20/80$) flow (Fig. 7). This means that the oxidation state of VO_x species in both the cases is close to +5. The high oxidation state of VO_x species in alkane-oxygen mixture had been previously observed in ethane [10,40] and n-butane oxidation [10]. For the Ti-containing catalysts in our study, the UV/Vis spectrum in a C_3H_8-O_2 ($C_3H_8/O_2/Ne = 40/20/40$) flow differs from that in an O_2 ($O_2/Ne = 20/80$) flow due to an increase in the Kubelka–Munk function in the 600–800 nm range. Such a shifting indicates that the oxidation state of VO_x species slightly decreases, i.e. VO_x species over Ti-containing materials are more reduced than over V–TiSi-0 under the ODP conditions with O_2.

Another important result is the absence of significant differences in the UV/Vis spectra of V–TiSi-15, when the ODP reaction is performed with O_2 and N_2O indicating similar oxidation state of VO_x species under both the reaction conditions. Contrarily, the UV/Vis spectra of V–TiSi-0 in the $C_3H_8/O_2/Ne = 40/20/40$ and $C_3H_8/N_2O/Ne = 40/40/20$ flows differ strongly; the oxidation state of VO_x species is significantly lower in the presence of N_2O than of O_2. For the V–TiSi-1 and V–TiSi-6 catalysts, the difference between UV/Vis spectra in the $C_3H_8/O_2/Ne = 40/20/40$ and $C_3H_8/N_2O/Ne$ flows was smaller than for V–TiSi-0, but bigger than for V–TiSi-15. In other words, the difference in the oxidation state of VO_x species in the ODP reaction with O_2 and N_2O decreases with an increase in the Ti content in the support. These results together with the below results on the kinetics of oxidation (by O_2 and N_2O) and reduction (by C_3H_8) of VO_x species are discussed in Section 3.4 to explain the effect of titanium on the ODP catalytic performance in Figs. 5 and 6.

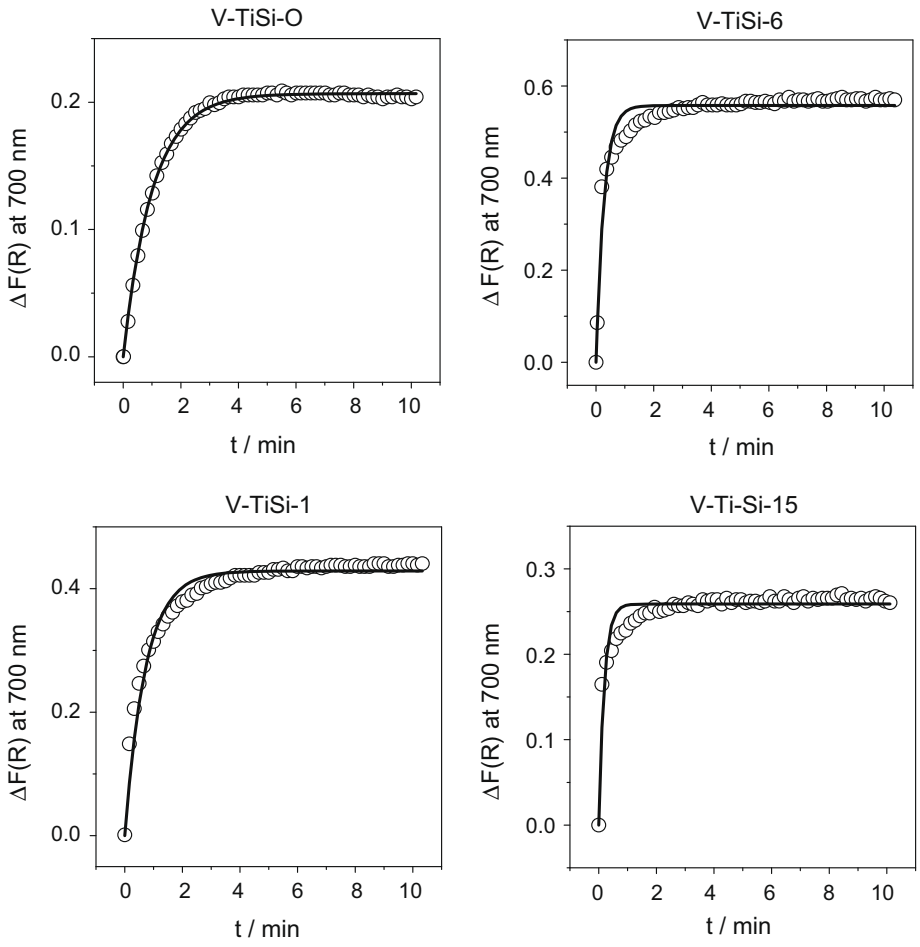

Fig. 8. Temporal changes in Kubelka–Munk function at 700 nm during reduction of fully oxidized VO_x species by C_3H_8 ($C_3H_8/Ne = 40/60$) at 773 K. Experimental data – not-filled circles, solid lines – simulated curves according to 1-site model (Eq. (4)). Catalyst was pretreated in O_2 flow ($O_2/Ne = 20/80$) at 773 K before the reduction.

3.3.2. Kinetics of reduction and reoxidation of VO_x species from time-resolved in situ UV/Vis analysis

The kinetics of reduction of oxidized VO_x species by C_3H_8 (and H_2) was derived from the analysis of temporal changes in the Kubelka–Munk function at 700 nm (Fig. 8). The experiments were performed as follows. We always started with fully oxidized samples. Therefore, the Kubelka–Munk function in the 600–800 nm range was zero, i.e. no reduced VO_x species. At time zero, we switched from an O_2 flow (O_2/Ne = 20/80) to a C_3H_8 flow (C_3H_8/Ne = 40/60). As a result, the Kubelka–Munk at 700 nm increases from 0 and reaches a constant value of. 0.2–0.6 after 4 min on C_3H_8 stream. It should be stressed that similar changes were observed, when H_2 was used as a reducing agent instead of C_3H_8. This important result additionally proves that the changes observed in the Kubelka–Munk function at 700 nm upon switching from O_2 to C_3H_8 are due to the reduction of VO_x species but not due to coke deposition. Propane conversion was <10%, and no temperature increase was detected in the catalyst bed during the course of the reduction. For quantifying the above-mentioned experiments, the experimental data were fitted to a simple kinetic model of reduction of VO_x species; the Kubelka–Munk function at 700 nm can be considered proportional to the concentration of reduced VO_x species. According to this model, propane reacts with an oxidized VO_x species yielding a reduced VO_x species:

$$C_3H_8 + VO_x(ox) \overset{K_1(C_3H_8)}{\rightarrow} C_3H_6 + CO_x + H_2O + VO_x(red) \quad (2)$$

This mechanistic scheme can be transformed into the following equation for the formation rate of reduced VO_x species:

$$\frac{dC(VO_x(red))}{dt} = K'_1(C_3H_8) \times C(VO_x(ox)) \quad (3)$$

where $K'_1(C_3H_8)$ is a product of the reaction constant ($K_1(C_3H_8)$) of reduction of VO_x species by propane and the partial pressure of propane, and $C(VO_x(ox))$ is the concentration of oxidized VO_x species in UV/Vis beam.

Integrating Eq. (3) results in the following expression for the time dependence of the concentration of reduced VO_x species assuming mass balance for the reduced and oxidized VO_x species:

$$C(VO_x(red)) = C^0(VO_x(ox)) \times (1 - \exp^{-K'_1(C_3H_8)\times t}) \quad (4)$$

where $C^0(VO_x(ox))$ is the total concentration of oxidized VO_x species, which participate in the reduction.

Eq. (4) was used for fitting the temporal changes in the Kubelka–Munk at 700 nm upon switching from O_2- to C_3H_8-containing flows at 773 K. The simulated responses are presented in Fig. 8 as solid lines. It is obvious that this simple model describes correctly the experimental data over the V–TiSi-0 material. However, the model fails to describe the experimental data over Ti-containing materials; the higher is the Ti loading, the worse is the description. It is important to highlight that this simple kinetic model does not also describe the kinetics of reduction of VO_x species over the Ti-containing catalysts by H_2. Taking into account the results of our H_2-TPR study in Fig. 4, it can be suggested that there are differently reducible VO_x species over Ti-containing materials. This figure clearly shows that there are at least two types of VO_x species over these catalysts. Therefore, we modified the kinetic model in Eq. (3) by assuming two differently reducible VO_x species. The corresponding rate equation for the formation of reduced VO_x species is:

$$\frac{dC(VO_x(red))}{dt} = K'_1(C_3H_8) \times C(VO_x(ox_1)) + K'_2(C_3H_8) \times C(VO_x(ox_2)) \quad (5)$$

This complex model describes the temporal changes in the Kubelka–Munk function over all the Ti-containing catalysts upon switching from O_2 to C_3H_8 (H_2). Fig. 9 shows for brevity the comparison between the experimental and calculated data over the V–TiSi-15 catalyst, where the worst description with the one-site model was achieved (Fig. 8). It is clearly seen that the 2-sites model describes the experimental results very well. The calculated kinetic parameters of reduction of VO_x species by C_3H_8 for the Ti-free and Ti-containing materials are summarized in Table 2. For the Ti-containing catalysts, $K'_1(C_3H_8)$ differs strongly from $K'_2(C_3H_8)$. Moreover, the $K'_1(C_3H_8)$ increases from 0.09 to 0.35 s^{-1} with increasing Ti content, while the $K'_2(C_3H_8)$ does not depend on the Ti loading and is similar for all the V–TiSi materials. Most probably, $K'_1(C_3H_8)$ and $K'_2(C_3H_8)$ are representatives for the reduction of VO_x bounded to Ti- and Si-containing species, respectively. This assumption is supported by the fact that the ratio of $C(VO_x(ox_1))/(C(VO_x(ox_1)) + C(VO_x(ox_2)))$ in Table 2 increases with an increase in the Ti loading. This ratio represents a portion of oxidized VO_x-(ox_1) species with respect to the total amount of oxidized VO_x species taking part in the reduction. Moreover, we suggest that Ti weakens the strength of V–O bond(s) in the VO_x species connected to TiO_x; the higher is the Ti content, the stronger is the effect on the bond strength. This is a possible reason for an increase in the $K'_1(C_3H_8)$ value.

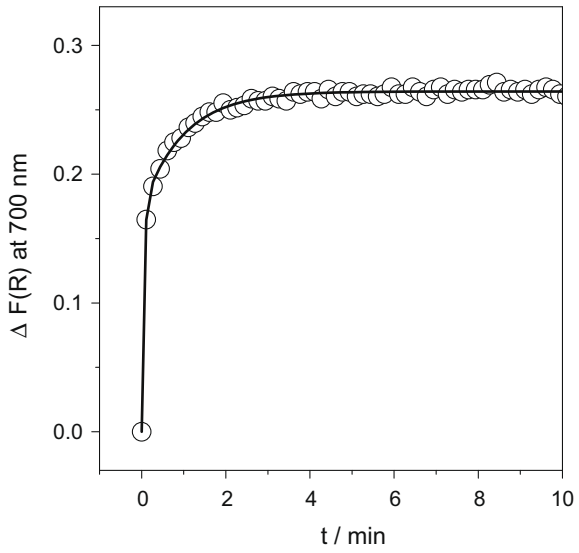

Fig. 9. Temporal changes in Kubelka–Munk function at 700 nm during reduction of fully oxidized VO_x species by C_3H_8 (C_3H_8/Ne = 40/60) of V–TiSi-15 at 773 K. Experimental data – not-filled circles, solid line – simulated curve according to 2-sites model (Eq. (5)). Catalyst was pretreated in O_2 flow (O_2/Ne = 20/80) at 773 K before the reduction.

The above fitting procedure was also used to quantitatively describe the kinetics of oxidation of reduced VO_x species by O_2 and N_2O. Similar to the reduction of VO_x species, one (Eq. (6)) and

Table 2
Kinetic parameters of reduction of fully oxidized VO_x species by C_3H_8 (C_3H_8/Ne = 40/60) determined by in situ UV/Vis spectroscopy at 773 K.

Sample	$C(VO_x(ox_1))/C(VO_x(ox))$[a]	$K'_1(C_3H_8)$ (s^{-1})	$C(VO_x(ox_2))/C(VO_x(ox))$[a]	$K'_2(C_3H_8)$ (s^{-1})
V–TiSi-0			1.0	0.017
V–TiSi-1	0.44	0.09	0.56	0.012
V–TiSi-6	0.72	0.14	0.28	0.012
V–TiSi-15	0.65	0.35	0.35	0.017

[a] The fitting parameters were $K'_1(C_3H_8)$, $K'_2(C_3H_8)$, $C(VO_x(ox_1))$, and $C(VO_x(ox_2))$. The ratios of $C(VO_x(ox_1))/C(VO_x(ox))$ and $C(VO_x(ox_2))/C(VO_x(ox))$ were calculated taking into account that $C(VO_x(ox)) = C(VO_x(ox_1)) + C(VO_x(ox_2))$.

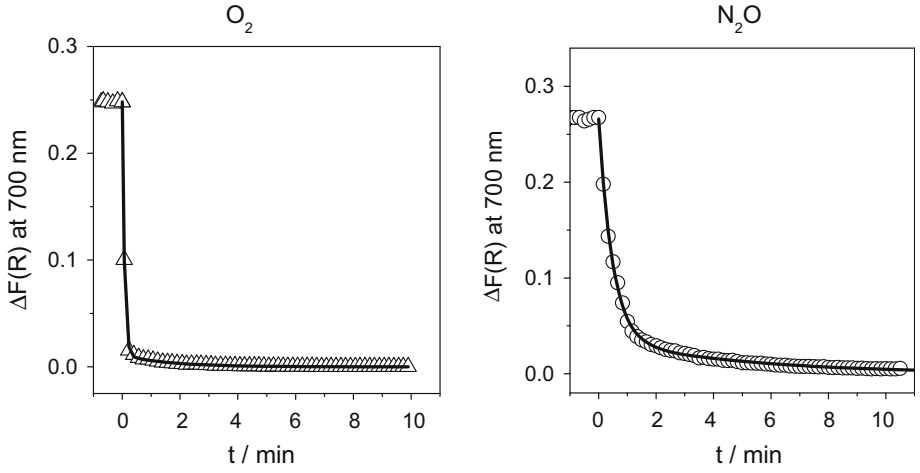

Fig. 10. Temporal changes in Kubelka–Munk function at 700 nm during oxidation of reduced VO_x species by O_2 (O_2/Ne = 20/80) and N_2O (N_2O/Ne = 40/60) of V–TiSi-15 catalyst at 773 K. Experimental data – not-filled symbols, solid line – simulated curve according to 2-sites model (Eq. (7)). Catalyst was pre-reduced in a C_3H_8/Ne = 40/60 flow for 20 min at 773 K before the oxidation.

two (Eq. (7)) types of reduced VO_x species were assumed for Ti-free and Ti-containing materials, respectively.

$$\frac{dC(VO_x(ox))}{dt} = K_1'ox \times C(VO_x(red_1)) \quad (6)$$

$$\frac{dC(VO_x(ox))}{dt} = K_1'ox \times C(VO_x(red_1)) + K_2'ox \times C(VO_x(red_2)) \quad (7)$$

where $K_i'ox$ is a product of the reaction constant of oxidation and the partial pressure of oxidant (O_2 or N_2O).

Fig. 10 compares the experimental data of catalyst reoxidation by O_2 and N_2O and the calculated ones over the V–TiSi-15 catalyst. It is clearly seen that the 2-sites model describes the experimental results well. The simulated kinetic parameters of oxidation of reduced VO_x species are summarized in Table 3 (oxidation by O_2) and Table 4 (oxidation by N_2O). For all the catalysts, oxygen reoxidizes reduced VO_x species faster than N_2O. However, the $K_1'(O_2)$ decreases, while the $K_1'(N_2O)$ increases with an increase in the Ti loading. The difference between O_2 and N_2O in the $C(VO_x(red_1))/C(VO_x(red))$ and $C(VO_x(red_2))/C(VO_x(red))$ ratios may be due to the different mechanisms of reoxidation of reduced VO_x species by O_2 and N_2O as reported in [41]. Moreover, the kinetics of catalyst reoxidation is very fast. Unfortunately, the applied UV/Vis spectrometer does not provide high enough time resolution for definitive discrimination between different reduced VO_x species under our experimental conditions.

In summary, the results of the above kinetic analysis enabled to define the following three effects of increasing Ti loading on the redox properties of surface VO_x species: (i) the constant of reduction of oxidized VO_x species increases significantly; (ii) the constant of oxidation of reduced VO_x species by O_2 decreases; and (iii) the constant of oxidation of reduced VO_x species by N_2O increases.

Table 3
Kinetic parameters of reoxidation of reduced VO_x species by O_2 (O_2/Ne = 20/80) determined by in situ UV/Vis spectroscopy at 773 K.

Sample	$C(VO_x(red_1))/C(VO_x(red))$[a]	$K_1'(O_2)$ (s^{-1})	$C(VO_x(red_2))/C(VO_x(red))$[a]	$K_2'(O_2)$ (s^{-1})
V–TiSi-0	1.0	0.70		
V–TiSi-1	0.97	0.45	0.03	0.01
V–TiSi-6	0.93	0.42	0.07	0.01
V–TiSi-15	0.96	0.23	0.04	0.01

[a] The fitting parameters were $K_1'(O_2)$, $K_2'(O_2)$, $C(VO_x(red_1))$, and $C(VO_x(red_2))$. The ratios of $C(VO_x(red_1))/C(VO_x(red))$ and $C(VO_x(red_2))/C(VO_x(red))$ were calculated taking into account that $C(VO_x(red)) = C(VO_x(red_1)) + C(VO_x(red_2))$.

Table 4
Kinetic parameters of reoxidation of reduced VO_x species by N_2O (N_2O/Ne = 40/60) determined by in situ UV/Vis spectroscopy at 773 K.

Sample	$C(VO_x(red_1))/C(VO_x(red))$[a]	$K_1'(N_2O)$ (s^{-1})	$C(VO_x(red_2))/C(VO_x(red))$[a]	$K_2'(N_2O)$ (s^{-1})
V–TiSi-0	1.0	0.019		
V–TiSi-1	0.91	0.025	0.09	0.001
V–TiSi-6	0.82	0.039	0.18	0.013
V–TiSi-15	0.85	0.035	0.15	0.003

[a] The fitting parameters were $K_1'(N_2O)$, $K_2'(N_2O)$, $C(VO_x(red_1))$, and $C(VO_x(red_2))$. The ratios of $C(VO_x(red_1))/C(VO_x(red))$ and $C(VO_x(red_2))/C(VO_x(red))$ were calculated taking into account that $C(VO_x(red)) = C(VO_x(red_1)) + C(VO_x(red_2))$.

3.4. Correlation of catalytic and spectroscopic data

The results of catalyst characterization and ODP tests as well as the kinetics of reduction and oxidation of highly dispersed VO_x species are discussed to explain the influence of Ti on the ODP reaction over VO_x(3.7 wt.%)/(Ti–Si)O_2. It should be stressed that the kinetic analysis was performed under controlled reaction conditions, which were very similar to those of our steady-state ODP tests. Therefore, a direct correlation between the catalytic (steady-state ODP activity) and kinetic parameters (obtained from time-resolved UV/Vis analysis) is possible. Two important effects of Ti should be especially mentioned: (i) the ODP activity increases with an increase in Ti loading using O_2 and N_2O (Fig. 6), and (ii) the difference in the propene selectivity between O_2- and N_2O-containing feeds decreases, when Ti loading increases (Fig. 5). It is known from [42] that Ti influences the acid–base properties of catalytic materials as well, and therefore may influence the catalytic performance. However, the activity of V-loaded samples in the ODP reaction was significantly higher compared to that of unloaded (Ti–Si)O_2 supports. Moreover, in the present contribution we discovered the differences in the catalytic performance of O_2 and N_2O in the ODP reaction (Fig. 5). These differences are influenced by Ti content in the supports. Since O_2 and N_2O do not change the acidic properties of the support, but influence the catalytic performance, we suggest that the support acidity should play a minor role. The redox properties of highly dispersed VO_x species should play an essential role in the ODP catalysis. The below discussion supports this suggestion.

Fig. 11 compares the constant of catalyst reduction by C_3H_8 with the TOF values obtained from the steady-state ODP catalytic tests using O_2 and N_2O as oxidizing agents. It is clearly seen that the higher is the constant, the higher are the TOF values for both the oxidants. For the ODP with O_2, the constant of reduction of VO_x species is very close to the TOF value for the corresponding samples. A similar observation was reported in [15] for the ODP reaction over VO_x/γ-Al_2O_3, where another UV/Vis approach was applied. In contrast to the ODP with O_2, the constant of reduction of VO_x species is significantly higher than the corresponding TOF value with N_2O. In [15], the ratio of the TOF value in the ODP to the constant of reduction derived from UV/Vis analysis was used for determining the fraction of active VO_x sites. If we apply this approach to our results, we get the fraction of 0.9 for the ODP with O_2 compared to that of 0.6–0.7 in [15]. This difference is related to the lower V surface densities (0.37–1.1 V/nm^2) in our samples, in which the existence of three-dimensional VO_x clusters can be excluded. When N_2O was used in the ODP reaction, the fraction of ca. 0.15 was determined for the V–TiSi-0, V–TiSi-1, and V–TiSi-6 materials, while it amounted to 0.5 for the V–TiSi-15 sample. This fact and the differences in the fraction of active sites between the ODP with O_2 and N_2O are due to the different kinetics of catalyst reoxidation by O_2 and N_2O (Tables 3 and 4).

Such a good correlation in Fig. 11 was derived because we performed the ODP and UV/Vis experiments under very similar conditions. It confirms also a Mars-van-Krevelen redox cycle involving lattice oxygen and reduced V^{3+} or V^{4+} centers. Thus, the increase in the ODP activity of $VO_x/(Ti–Si)O_2$catalyst is explained by an increase in the reducibility of VO_x species with increasing Ti content in the support.

We compare the ratio of $K'_i(C_3H_8)/K'_1(O_2)$ as a function of Ti content in the support to explain the influence of Ti in VO_x(3.7 wt.%)/$(Ti–Si)O_2$ on propene selectivity in the ODP reaction with N_2O and O_2. This ratio determines the reduction degree of the catalysts; the higher the ratio, the higher the reduction degree. Fig. 12a illustrates that this ratio increases with an increase in the Ti content. Since the $K'_i(C_3H_8)/K'_1(O_2)$ ratio determined over V–TiSi-0 and V–TiSi-1 is significantly lower than 1, it can be concluded that VO_x species over these samples should be mainly in their highest oxidation state during the course of the ODP reaction. This agrees well with our steady-state in situ UV/Vis data in Fig. 7 and with literature data [10,40]. Contrarily, the $K'_i(C_3H_8)/K'_1(O_2)$ ratio over V–TiSi-15 is greater than 1 indicating that VO_x species over this catalyst should be reduced under the ODP conditions. This theoretical conclusion is supported by the results of our steady-state in situ UV/Vis experiments in Fig. 7, where no significant differences in the

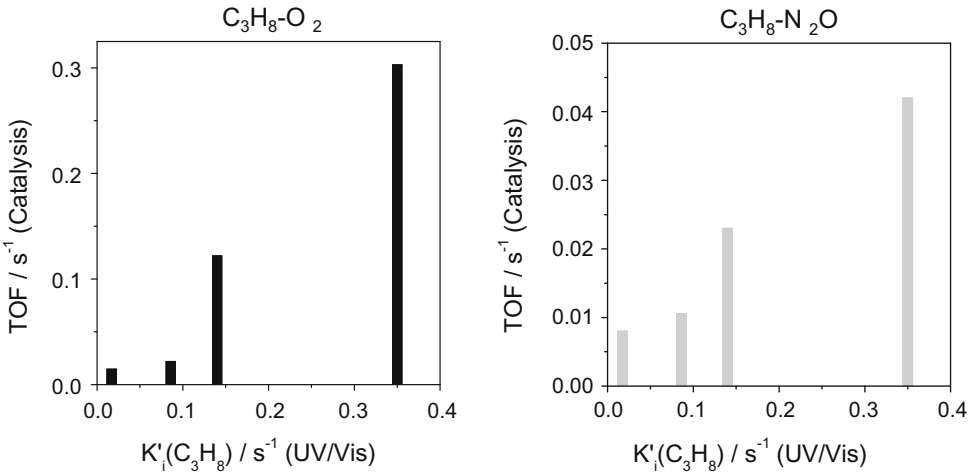

Fig. 11. Comparison of the constants of reduction of fully oxidized VO_x species by C_3H_8 from UV/Vis measurements with the TOF values obtained in the catalytic ODP experiments with O_2 and N_2O at $T = 773$ K. $i = 2$ and $i = 1$ in the $K'_i(C_3H_8)$ from Table 2 are for Ti-free and Ti-containing samples, respectively.

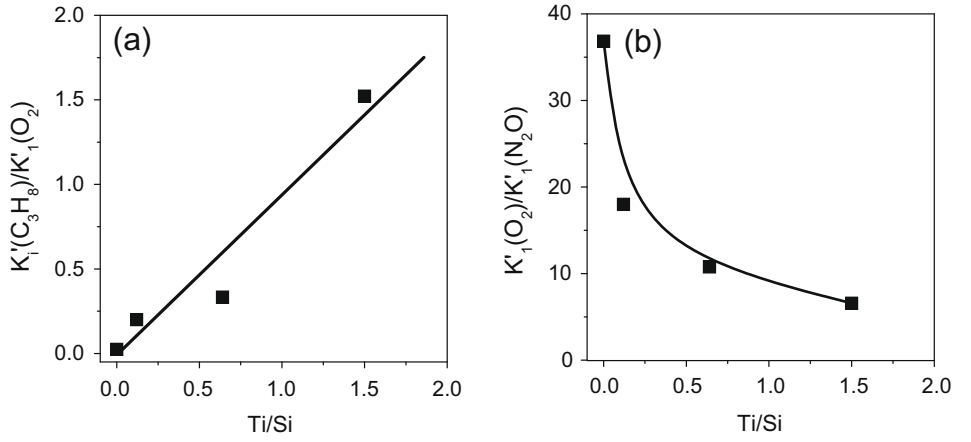

Fig. 12. The ratios of $K'_i(C_3H_8)/K'_1(O_2)$ (a) and of $K'_1(O_2)/K'_1(N_2O)$ (b) from Tables 3 and 4 as a function of Ti/Si ratio. $i = 2$ and $i = 1$ in the $K'_i(C_3H_8)$ from Table 2 are for Ti-free and Ti-containing samples, respectively.

UV/Vis spectra of V–TiSi-15 under the ODP conditions with O_2 and N_2O are seen.

Fig. 5 demonstrates that the difference in the propene selectivity between O_2- and N_2O-containing feeds decreases with an increase in Ti loading. This effect can be explained as follows. The constant of reduction of oxidized VO_x species by C_3H_8 ($K'_i(C_3H_8)$) increases (Table 2) with Ti loading. However, the ratio of $K'_1(O_2)/K'_1(N_2O)$. Decreases from ca. 37 to ca. 6.6 with increasing the Ti/Si ratio from 0 to 1.5 (Fig. 12b). In other words, the difference in the oxidizing ability of O_2 and N_2O for the reoxidation of reduced VO_x species decreases with Ti loading. Therefore, the difference in the oxidation degree of VO_x species under the ODP conditions with O_2 and N_2O over VO_x(3.7 wt.%)/(Ti–Si)O_2 should also decrease with Ti loading. This theoretical conclusion is well supported by the results of in situ UV/Vis analysis under steady-state ODP conditions in Fig. 7. This figure demonstrates that the differences in the UV/Vis spectra of VO_x(3.7 wt.%)/(Ti–Si)O_2 between O_2- and N_2O-containing ODP feeds decrease, when Ti loading increases. Taking into account the effects of Ti loading on the reduction degree of VO_x species and their ODP performance with O_2 and N_2 in Fig. 5, it is suggested that the reduction degree determines the propene selectivity.

The results obtained evidence that time-resolved operando UV/Vis spectroscopy is a promising technique to study the reduction-oxidation kinetics of supported transition metal oxides. In conventional kinetic studies, one usually follows the concentration of a reagent or a product with time, normally it proceeds with a certain time delay even when the fast analytic methods are applied. With in situ UV/Vis methods the transition metal ions are probed directly. Since the UV/Vis experiments are performed with a high time resolution, fast redox reaction processes can be easily measured. Thus, UV/Vis spectroscopy can be complementary to conventional kinetic techniques [13].

4. Conclusions

The present contribution highlights the potential of in situ UV/Vis technique operating under steady-state and transient conditions for analyzing the reduction degree of highly dispersed transition metal oxide aggregates as well as for deriving the kinetic parameters of their reduction and oxidation. In order to avoid misinterpreting in situ UV/Vis results, it is highly important to thoroughly control reaction conditions (temperature, feed composition, degree of conversion). UV/Vis analysis under steady-state conditions of the oxidative dehydrogenation of propane enabled to conclude that the reduction degree of highly dispersed VO_x species over Ti–Si-MCM-41 (Ti/Si = 0–1.5) catalytic materials is an important factor for achieving high propene selectivity. The reduction degree can be tuned by oxidizing agents (O_2, and N_2O) and by the ratio of Ti/Si in the support; the higher is the ratio, the higher is the reduction degree.

Possible mechanistic origins of the influence of Ti on the ODP performance were derived from transient kinetic UV/Vis analysis. This analysis in combination with H_2-TPR enabled to identify at least two differently reducible VO_x species upon incorporation of titanium into silica support. The presence of Ti in the support increases the reducibility of VO_x species. A near to linear correlation between the kinetic parameters of reduction of VO_x species by C_3H_8 and the catalyst activity for propane conversion was established. Titanium decreases the ability of reduced VO_x species for reoxidation by O_2, but slightly increases by N_2O.

Acknowledgment

Support by Deutsche Forschungsgemeinschaft (DFG) within the frame of the competence network (Sonderforschungsbereich 546) "Structure, dynamics and reactivity of transition metal oxide aggregates" is greatly appreciated.

References

[1] B.M. Weckhuysen, Chem. Commun. (2002) 97.
[2] R.L. Puurunen, B.G. Beheydt, B.M. Weckhuysen, J. Catal. 204 (2001) 253.
[3] X. Gao, I.E. Wachs, J. Phys. Chem. B 104 (2000) 1261.
[4] M.D. Argyle, K. Chen, A.T. Bell, E. Iglesia, J. Catal. 208 (2002) 139.
[5] M.D. Argyle, K. Chen, C. Resini, C. Kebs, A.T. Bell, E. Iglesia, J. Phys. Chem. B 108 (2004) 2345.
[6] L. Burcham, G. Deo, X. Gao, I.E. Wachs, Top. Catal. 11/12 (2000) 85.
[7] X. Gao, J.-M. Jehng, I.E. Wachs, J. Catal. 209 (2002) 43.
[8] A. Brückner, E.V. Kondratenko, Catal. Today 113 (2006) 16.
[9] B.M. Weckhuysen, D.E. Keller, Catal. Today 78 (2003) 25.
[10] X. Gao, M.A. Bañares, I.E. Wachs, J. Catal. 188 (1999) 325.
[11] O. Ovsitser, M. Cherian, E.V. Kondratenko, J. Phys. Chem. C 111 (2007) 8594.
[12] E.V. Kondratenko, O. Ovsitser, J. Radnik, M. Schneider, R. Kraehnert, U. Dingerdissen, Appl. Catal. A 319 (2007) 98.
[13] A. Bensalem, B.M. Weckhuysen, R.A. Schoonheydt, J. Phys. Chem. B 101 (1997) 2824.
[14] G. Grubert, J. Rathousky, G. Schulz-Ekloff, M. Wark, A. Zukal, Micropor. Mesopor. Mater. 22 (1998) 225.
[15] M.D. Argyle, K. Chen, E. Iglesia, A.T. Bell, J. Phys. Chem. B 109 (2005) 2414.
[16] U. Bentrup, A. Brückner, M. Fait, B. Kubias, J.B. Stelzer, Catal. Today 112 (2006) 78.
[17] J.J. Bravo-Suárez, K.K. Bando, T. Fujitani, S.T. Oyama, J. Catal. 257 (2008) 32.
[18] J.J. Bravo-Suárez, K.K. Bando, J. Lu, M. Haruta, T. Fujitani, S.T. Oyama, J. Phys. Chem. C 112 (2008) 1115.
[19] M. Kobayashi, R. Kuma, S. Masaki, N. Sugishima, Appl. Catal. B 60 (2005) 173.
[20] C.R. Dias, M.F. Portela, M.A. Bañares, M. Galan-Fereres, M. Lopez-Granados, M.A. Pena, Appl. Catal. A 224 (2002) 141.
[21] N.E. Quaranta, J. Soria, V.C. Corberan, J.L.G. Fierro, J. Catal. 171 (1997) 1.
[22] A. Comite, A. Sorrentino, G. Capannelli, M. Di Serio, R. Tesser, E. Santacesaria, J. Mol. Catal. A 198 (2003) 151.
[23] E.A. Mamedov, V.C. Corberan, Appl. Catal. A 127 (1995) 1.
[24] M.A. Bañares, X. Gao, J.L.G. Fierro, I.E. Wachs, Stud. Surf. Sci. Catal. 110 (1997) 295.
[25] B.M. Weckhuysen, Phys. Chem. Chem. Phys. 5 (2003) 4351.
[26] E.V. Kondratenko, M. Cherian, M. Baerns, Catal. Today 112 (2006) 60.
[27] E.V. Kondratenko, M. Cherian, M. Baerns, X. Su, R. Schlögl, X. Wang, I.E. Wachs, J. Catal. 234 (2005) 131.
[28] D.M. Pickup, G. Mountjoy, G.W. Wallidge, R. Anderson, J.M. Cole, R.J. Newport, M.E. Smith, J. Mater. Chem. 9 (1999) 1299.
[29] G. Kortüm, Reflexionsspektroskopie, Springer Verlag, Berlin, 1968. p. 187.
[30] T. Blasco, J.M. López Nieto, Appl. Catal. A 157 (1997) 117.
[31] S. Gontier, A. Tuel, Micropor. Mater. 5 (1995) 161.
[32] C.-B. Wang, G. Deo, I.E. Wachs, J. Catal. 178 (1998) 640.
[33] I.E. Wachs, Catal. Today 27 (1996) 437.
[34] C.-B. Wang, Y. Cai, I.E. Wachs, Langmuir 15 (1999) 1223.
[35] N. Magg, B. Immaraporn, J.B. Giorgi, T. Schroeder, M. Bäumer, J. Döbler, Z. Wu, E. Kondratenko, M. Cherian, M. Baerns, P.C. Stair, J. Sauer, H.-J. Freund, J. Catal. 226 (2004) 88.
[36] M.M. Koranne, J.G. Goodwin, G. Marcelin, J. Catal. 148 (1994) 369.
[37] F. Arena, N. Giordano, A. Parmaliana, J. Catal. 167 (1997) 66.
[38] X. Gao, S.R. Bare, J.L.G. Fierro, I.E. Wachs, J. Phys. Chem. B 103 (1999) 618.
[39] H.-M. Lin, S.-T. Kao, K.-M. Lin, J.-R. Chang, S.-G. Shyu, J. Catal. 224 (2004) 156.
[40] M.A. Bañares, M.V. Martinez-Huerta, X. Gao, J.L.G. Fierro, I.E. Wachs, Catal. Today 61 (2000) 295.
[41] X. Rozanska, E.V. Kondratenko, J. Sauer, J. Catal. 256 (2008) 84.
[42] P. Ratnasamy, D. Srinivas, H. Knözinger, Adv. Catal. 48 (2004) 1.